Solar Energy 320 (2026) 115211

Contents lists available at ScienceDirect

Solar Energy

journal homepage: www.elsevier.com/locate/solener

Wind effects on convective losses from a rotating cavity solar receiver

Onur Polat [a,*], Luka Lackovic [a], Reiner Buck [a], Robert Pitz-Paal [a,b], Harald Kruggel-Emden [c]

[a] German Aerospace Center, Institute of Solar Research, Germany
[b] RWTH Aachen University, Chair of Solar Technology, Linder Höhe, Köln, 51147, Germany
[c] Chair of Mechanical Process Engineering and Solids Processing, Technische Universität Berlin, Ernst-Reuter-Platz 1, Berlin, 10587, Germany

ARTICLE INFO

Handling Editor: XXXXXXXX

Keywords:
Concentrating solar thermal
Cavity receiver
Convection
Rotation
Wind
CFD

ABSTRACT

Solar particle receivers are considered a promising option for high temperature solar power and process heat applications. This paper aims to demonstrate the effects of rotation speed, wind speed, wind direction and receiver tilt on thermal losses via convection from a rotating, cylindrical cavity particle receiver. CFD simulations for a full-size receiver with a housing and tower were performed for this purpose. Wind speeds of 0, 2, 7, 15 and 25 m/s, blowing from all directions resolved in 10° intervals were considered. The receiver was tilted 22.5°, 30°, 37.5° and 45° downward. The results show that regardless of wind speed and direction, rotation leads to a more than 20 % increase in convective losses. Moreover, convective losses vary with wind direction in a manner that cannot be described by interpolating between front and side winds. For some wind directions and receiver tilts, convection becomes the primary mode of heat loss. Air flow in and out of the cavity is analyzed in detail for these cases and the effect of the sense of rotation is explained.

1. Introduction

Concentrating solar thermal (CST) technologies combined with relatively cheap thermal storage options allow different hybridization strategies with other sources to offer renewable energy around the clock [1–3]. For low to medium temperature applications up to 500°C, line focus systems offer proven solutions with high technological readiness level (TRL) [4] whereas point-focus systems are necessary for attaining higher temperatures [5]. Dish and Scheffler systems with smaller receivers offer modular systems that can be realized with limited budget for low-cost applications in underdeveloped regions to supply solar heat [6]. Due to the modular nature of these systems, MW-scale installations suffer from higher losses, limiting their peak temperature and efficiency. On the other hand, tower systems with a single, large receiver can reach temperatures above 1000°C to supply high temperature heat for electricity production or industrial processes [7,8].

At high receiver surface temperatures radiative losses which are proportional to the fourth power of surface temperature becomes a serious problem. By assembling the receiver surfaces in the form of a cavity, view factor to the environment, and therefore radiative losses, can be reduced [8]. The downside is that heliostat field must be confined within a limited angle instead of surrounding the tower.

Another challenge for reaching higher temperatures is the very limited choice of materials for the receiver and heat transfer medium (HTM) [8]. The most promising HTM is ceramic particles which can be heated directly by concentrated sunlight [9]. In falling particle receivers (FPRs), particles move under the influence of gravity and flow speed is controlled by either stair-steps or protrusions into the particle stream [9]. FPRs have only a few moving parts, reducing the number of failure points. However, maintaining a thin but opaque curtain is difficult even at design power [10,11]. Therefore, FPRs are difficult to operate when solar input is significantly below design conditions.

In order to address the opacity problems while maintaining operational flexibility under a wide range of incident power at the aperture, researchers from the German Aerospace Center (DLR) propose the centrifugal receiver (CentRec) [9,12]. It is essentially a fast-rotating, down-tilted cylinder for heating particles as they flow along the side wall at the top of rotation. The key aspects of CentRec and a picture of a real unit is presented in Figs. 1a and 1b respectively.

As the receiver rotates, particles accelerate in tangential direction when the threshold of friction force is less than the wall-parallel

Abbreviations: CCW, Counterclockwise; CW, Clockwise; d_{ap}, Aperture diameter [m]; g, Gravity [m/s^2]; IDDES, Improved delayed detached eddy simulation.; L, Distance from the back plate [m]; l_c, Characteristic length [m]; Gr, Grashof number; Pr, Prandtl number; Ra, Rayleigh number; RANS, Reynolds-averaged Navier-Stokes; Re, Reynolds number; rpm, Rotations per minute; T, Temperature [K]; V_{wind}, Wind speed [m/s]; y^+, Dimensionless wall distance.

* Corresponding author.
E-mail address: onur.polat@dlr.de (O. Polat).

https://doi.org/10.1016/j.solener.2026.115211
Received 1 June 2026; Received in revised form 12 September 2026; Accepted 4 October 2026
Available online 21 October 2026
0038-092X/© 2026 The Author(s). Published by Elsevier Ltd on behalf of International Solar Energy Society. This is an open access article under the CC BY license (http://creativecommons.org/licenses/by/4.0/).
Open access funding enabled and organized by Projekt DEAL.

Nomenclature

Greek Symbols

α	Wind direction [°]
β	Coefficient of volume expansion [1/K]
Δ	Difference
θ	Receiver tilt [°]
ν	Kinematic viscosity [m^2/s]
ω	Rotation speed [rpm]

Subscripts

c	Characteristic
ap	Aperture
cav	Cavity
conv	Convection
rad	Radiation
rel	Relative

thickness around 10-15 particle diameters, forming a surface that is mostly impervious to the air [13,14]. Therefore, convective losses from the receiver can be approximated as losses from a rotating cavity with solid walls.

First studies concerning the convective losses from large cavity receivers were focused on natural convection. Clausing [15] theorized that a pocket of hot air called the stagnant zone forms above the plane normal to the gravity vector and above the topmost point of aperture, shielding the surfaces touching this pocket from the outside. The region below is called the convective zone. Convective heat transfer is assumed to take place only from the surfaces below this plane. In following works, he and his coworkers refined their theory and proposed a Nusselt (Nu) number correlation encompassing laminar, mixed and turbulent free convection regimes [16] and verified it [17]. They concluded that the position, orientation and size of the aperture are critical factors for convection from cavity receivers. With its theoretical basis and accurate experimental data used to determine the empirical constants, this correlation shows remarkable accuracy across different receiver designs. In order to accommodate tilted receivers, using the sum of the aperture length and its vertical projection has been proposed. Later studies

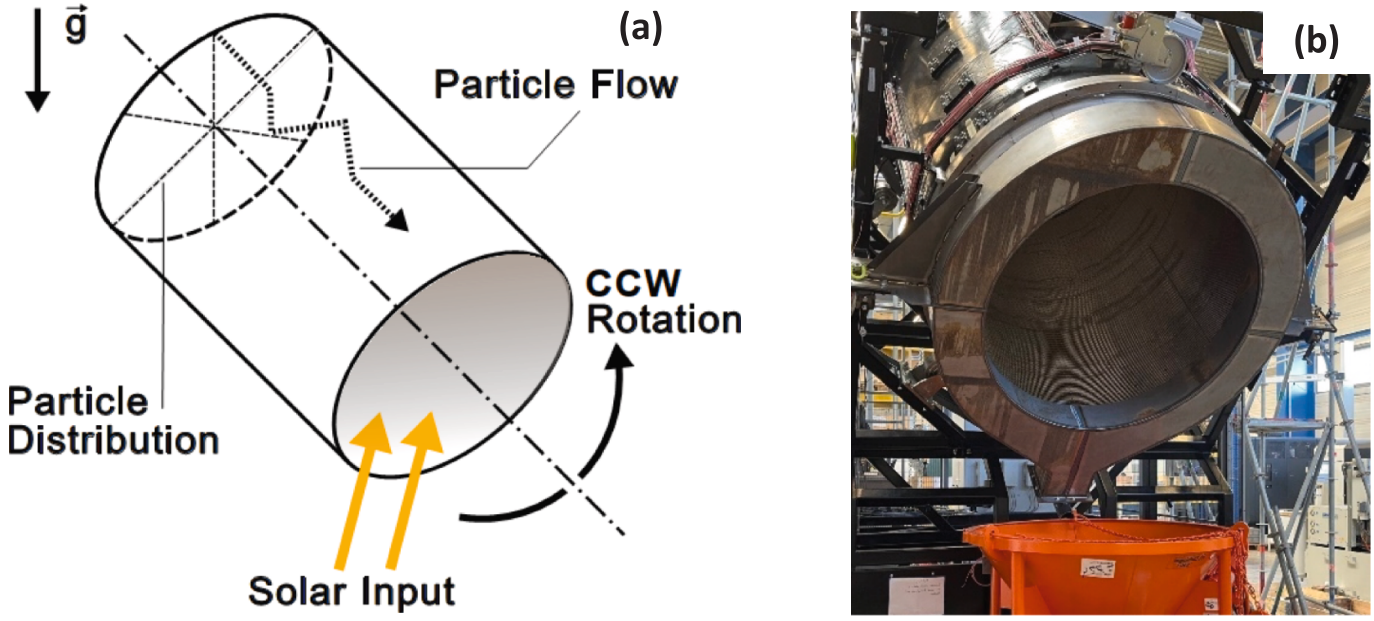


Fig. 1. a) Operation principle of centrec, rotating counterclockwise. b) A CentRec unit without the receiver housing.

component of the gravity vector and vice versa. The resulting motion of particles follows a zig-zag pattern. The duration of motion per turn depends on the rotation speed. This in turn allows adjusting the particle residence time by fine tuning the rotation speed in a range of 1-2 rpm. Meanwhile, the particle film on the wall remains almost packed with a

[18,19] have confirmed the shape of flow in and out of the receiver using visualization techniques. Abbasi-Shavazi et al. [20] have extended this theory to non-uniform wall temperatures and cylindrical receivers. Despite being derived using a small test unit, their correlation agrees well with the correlation from Clausing et al. [16] for a wide range of

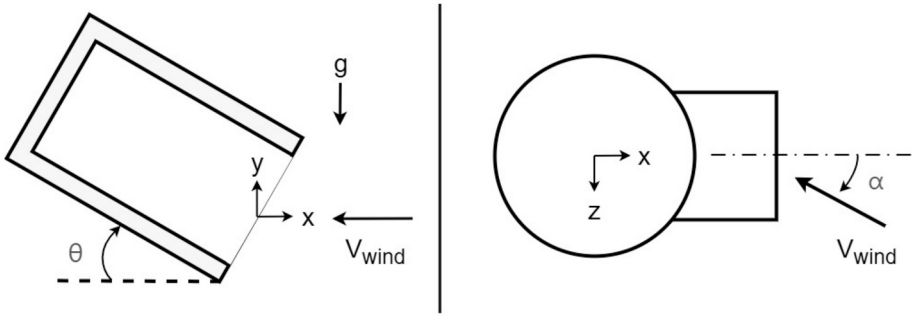


Fig. 2. Receiver tilt and wind direction.

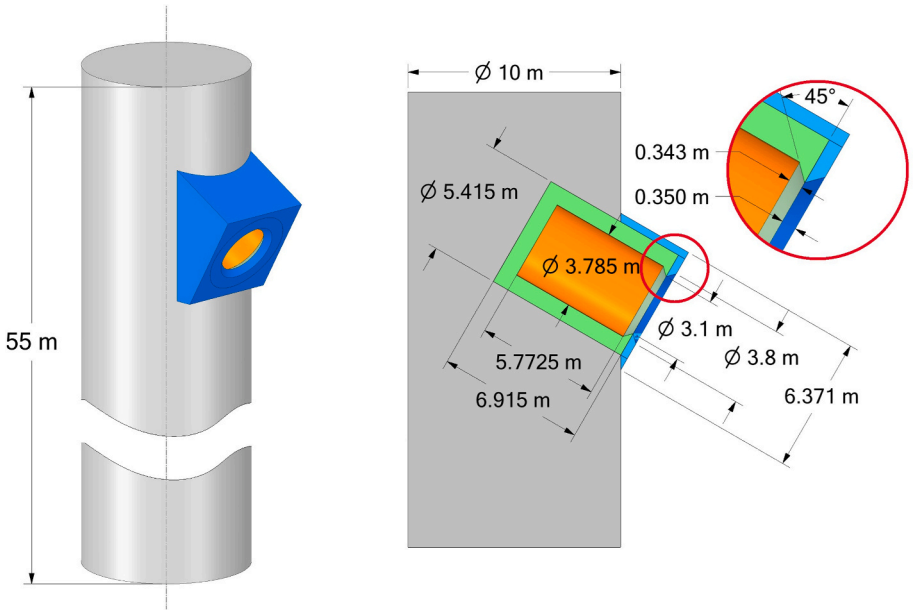


Fig. 3. Receiver shape and dimensions for the 30-degree tilt.

Rayleigh (Ra) numbers for isothermal cavities.

Contrary to the claims in early studies [21] wind at the top of the towers is strong enough to affect thermal losses due to convection [22,23]. Therefore, the effect of wind speed and direction has to be taken into account as well. Receiver orientation relative to the wind is usually described by the two angles shown in Fig. 2. The tilt angle (θ) describes how much the aperture plane normal is below horizontal. In this paper, wind direction (α) is zero degrees for the "head-on" and increases when direction goes clockwise when viewed from the top.

Researchers agree that increasing wind speed usually increases convective losses [24,25]. If the receiver design helps to direct the wind from top to bottom – for example a large, tilted front panel around the aperture – it is possible to reduce convective losses below free convection levels [26]. Other experimental works [27–29] confirmed that for some wind directions, convective losses increase significantly and structural alterations on receiver housing can address these spikes. In addition to the constant wind speed and direction, Ho et al. [30] investigated gusts as well. They concluded if the speed change persists for more than eight seconds, steady-state conditions are re-established.

Since CentRec is a relatively new concept, there are no publications on thermal losses from a rotating cavity solar receiver except one. Wu et al. [31] have used a small-scale test setup (D = 0.158 m, L = 0.245 m, $\omega \leq 150$ rpm) to investigate the effect of rotation on free convection. They concluded the effect of rotation is within 10%, corresponding to a negligible 1% on thermal efficiency. However, their setup had Ra = [8.46, 15.9] × 10^6, which is different from values for larger units. For large scale receivers, there are no experimental or numerical studies.

In this paper, we will investigate the variation of convective losses from a full-size CentRec with different tilts under various wind velocities. In addition to showing which wind directions lead to highest losses, phenomena causing the increase will be investigated in detail. As there is no relevant experimental data in the literature for large receivers, we verified our simulations using correlations for free convection instead.

2. Simulation Geometry

Since the structures around the receiver are known to affect convective losses the housing and the tower section around the receiver must be included in the model. However, our simulations are not related to a unit that has been built. Instead, the receiver size was derived from current limitations for road transport of factory-built receivers under highway bridges. Per Road Traffic Licensing Regulations of Germany (StVZO) section 32 [32], the maximum loaded height of a vehicle may

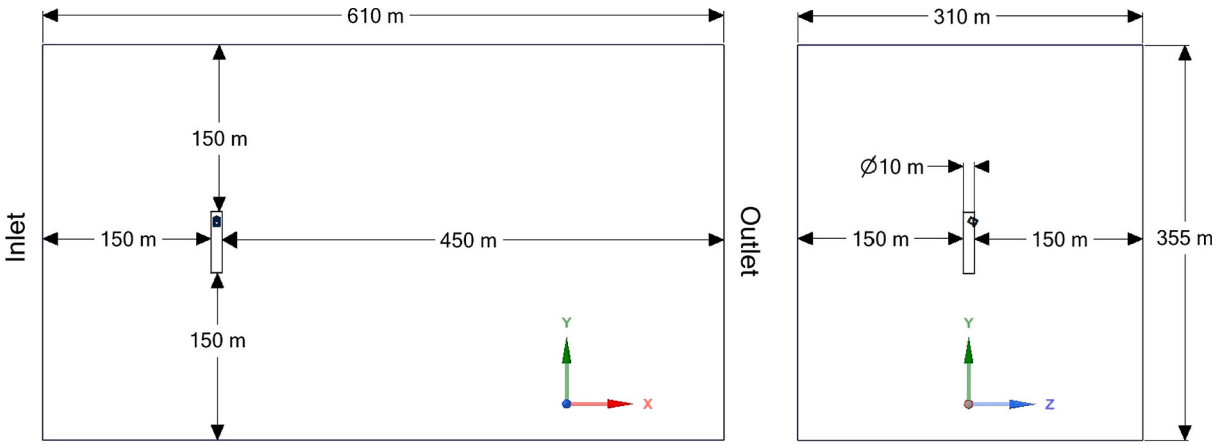


Fig. 4. Sketch of the simulation domain with key dimensions.

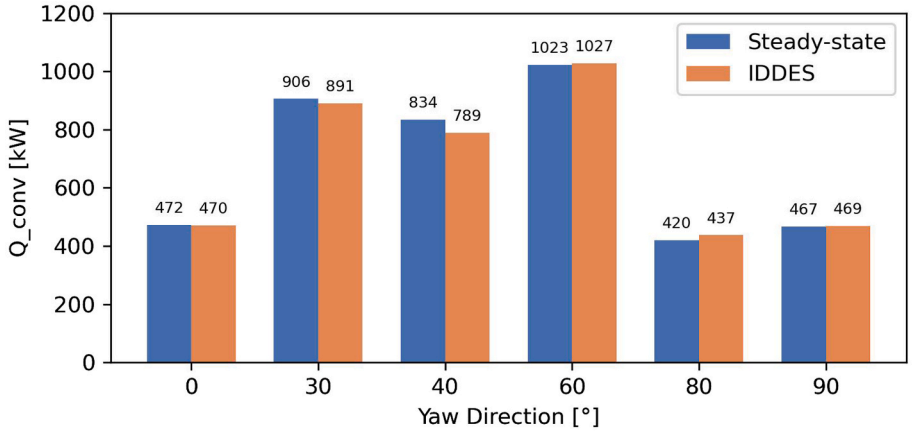


Fig. 5. Comparison between IDDES and steady-state simulations for $\theta = 22.5°$ and $V_{wind} = 25$ m/s.

not exceed 4.00 m and bridge heights are around 5 m [33]. Consequently, the largest receiver and frame assembly that can be safely transported under the bridges has an aperture diameter of 3.1 m. Other dimensions were then scaled up from the concepts explored in former research [12,28]. The dimensions used in the simulations are depicted in Fig. 3.

The receiver has 3.1 m aperture diameter, with the cavity having 3.8 m inner diameter and 5.8 m length. The lower edge of the receiver is at the edge of the tower. The prismatic housing with a flat radiation shield is selected to enlarge the stagnation zone in front of the aperture. Finally, only the top 55 m of the tower was considered in the simulation to reduce the computational effort. As depicted in Fig. 4, the whole structure is enclosed in a box whose faces were 150 m away from the structure in the upstream, sideways and vertical directions while the downstream face was 450 m away to ensure the boundaries are far enough to have negligible effect on the flow. The enclosure was aligned with the wind with one inlet and one outlet. Side surfaces were assumed to be walls. The effect of wind direction was evaluated by rotating the tower with the receiver inside the box.

3. Methodology

3.1. Modelling Flow and Heat Transfer

The focus of this work is to understand the effects of wind speed and direction on convective losses from a solar receiver using numerical methods. The number of cases to be simulated is therefore relatively high. In order to achieve reasonable computation times, models with just enough resolution had to be selected. Former numerical studies on cavity receivers have successfully demonstrated that two-equation turbulence models, namely the k-ω and k-ε families, and steady-state simulations yield adequate results [34,35].

The k-ω SST method combines the k-ε model in the far-field and standard k-ω model close to walls using a blending function [36]. This avoids the free stream sensitivity of the standard k-ω model while maintaining its superior performance in regions close to the walls. Moreover, it offers superior performance in flows involving adverse pressure gradients and separation. Since its inception in 1994, the k-ω SST model has been employed with great success in various areas such as design of turbomachinery, wind turbines and vehicles [37,38]. Our preliminary benchmarking analyses on free convection in rectangular prism enclosures and mixed convection from an isothermal cylinder in cross flow have also shown that the k-ω SST turbulence model and steady-state simulations gave results that matched the experiments and improved delayed detached eddy simulations (IDDES) closely and more so than other two-equation models.

In addition to reduction in computational workload by performing steady-state simulations, the implementation of the k-ω SST model in Fluent allows for y^+ insensitive wall treatment with wall functions, which reduces the mesh resolution requirements and offers the possibility to model wall roughness using the sand grain model [39]. The air surrounding the receiver is assumed to be at atmospheric pressure with temperature-dependent properties modelled using piecewise polynomials fitted to data from literature [40].

We compared the steady-state RANS and time-dependent IDDES simulations using the predicted convective heat loss for $\theta = 22.5°$ and $V_{wind} = 25$ m/s for $\alpha \in \{0, 30, 40, 60, 80, 90\}$ degrees. These analyses were performed after completing all steady-state simulations. Therefore, the wind directions are selected to represent different flow conditions observed. Each individual case took one day to simulate. The results for the steady-state and IDDES simulations are compared in Fig. 5.

Clearly, all cases show remarkable agreement, suggesting that the extra effort does not yield any meaningful difference. Therefore, we concluded the steady-state RANS simulations are enough for the problem in hand.

Test experience with CentRec so far has shown minimal dust formation in the receiver, supporting the assumption of non-participating media for the air in and around the receiver. Also, the particles form a quasi-packed layer in which contact is maintained even when particles are flowing. Therefore, incident rays have negligible penetration [41]. Finally, the particles have rather uniform properties in the wavelength ranges of interest [42]. Based on these reasons, we concluded the surface-to-surface radiative heat transfer model with diffuse and grey surfaces will be adequate to approximate radiative heat transfer between surfaces constituting the domain.

3.2. Boundary conditions

CST receivers are used to heat an HTM. Therefore, the receiver surfaces are expected to have spatial temperature variations as the fluid runs through the receiver. The target for the next generation CentRec receiver is to achieve a particle outlet temperature of 1000°C from an inlet temperature of 200°C. IR camera results from on-sun inliner performance tests have shown that temperature increases almost linearly from the particle inlet at the back plate of the receiver towards aperture. We approximated this using a prescribed temperature boundary condition on the side walls of the cavity given in equation (1). Unfortunately, the quality of the temperature measurements and lack of recorded wind data prohibited exploiting the readings from these tests as verification data.

$$T_{cav,side} = \frac{(1273 - 853)[K]}{5.7725[m]} L + 853[K] \quad (1)$$

Here, L is the distance along the cylinder axis, measured from the back

Table 1
Parameter space.

Wind speed	0, 2, 7, 15 and 25 m/s
Wind direction	[0°, 360°] in 10° increments
Receiver tilt	22.5°, 30°, 37.5° and 45°
Rotation speed	0 and 30 rpm

plate. The back plate is assigned a uniform temperature of (1273 + 853)/2 = 1063 K, again based on IR images. The surroundings are assumed to be at 300 K. All other surfaces were assumed to be adiabatic.

For the radiation exchange model, receiver surfaces are assigned a total hemispherical emissivity of 0.8, reflecting the average of the values reported in the literature [43–46]. The receiver housing was assumed to be made from a diffuse reflective insulation material with a total hemispherical emissivity of 0.05 [47]. The tower is assumed to be made out of concrete with 0.5 emissivity [48]. Surroundings are modelled as black and isothermal surfaces of the enclosure at 300 K.

Rotation is modelled using prescribed velocities on side and back walls of the cavity. Ideal rotation speed for a particle receiver is determined for a small test unit tilted 45°, which is then scaled up to the receiver based on forces acting on the particle as it rotates with the receiver. For the given dimensions, this corresponds to 30 rpm. For other tilts, an estimate was made, again using the magnitude of forces acting on particles around one rotation.

3.3. Parameters of Interest

In this study, we focus on effects of wind speed and wind direction for a rotating cavity receiver. To do so, we have focused on the parameters listed in Table 1. In order to keep the number of simulations reasonable, we did not consider variable size and shape for the receiver, tower and housing. The only structural parameter is the receiver tilt, which determines the angle between the wind and the aperture.

The dimensionless groups corresponding to these parameters are calculated using the average wall temperature of the cavity and the temperature of the surroundings as reference values. The characteristic length (l_c) is given by equation (2) as follows:

$$l_c = d_{ap}(1 + \cos\theta) \tag{2}$$

The maximum Reynolds number is then calculated using the maximum wind speed and lowest tilt as:

$$Re = \frac{V_{wind} l_c}{\nu} = \frac{25(3.1(1 + \cos(22.5^\circ)))}{6.477 \times 10^{-5}} = 2.30 \times 10^6 \tag{3}$$

Buoyancy is characterized by the Grashof number (Gr). It can be interpreted as the square of buoyancy speed made dimensionless as well. For our simulations Gr is calculated as:

$$Gr = \frac{g\beta(T_{hot} - T_{cold}) l_c^3}{\nu^2} \tag{4}$$

It ranges between [3.88, 5.55]·10^{11}. The relative strength of buoyancy and wind in convection is described by the Richardson number ($Ri = Gr/Re^2$). The cases investigated in this paper have $Ri \geq 0.1$, indicating both buoyancy and wind effects are important.

Rotation Reynolds number is defined using the tangential speed of the side walls. If $V_{wall} = \omega \cdot d_{cav}/2 = 5.945$ m/s, then for the 30° tilt $Re_{rot} = 5.31 \times 10^5$ which corresponds to $Ri_{rot} = 1.80$. This indicates rotation at 30 rpm can have a significant impact on convective losses. In this paper, we define the sense of rotation as counter-clockwise (CCW) as seen by a viewer looking into the cavity from the outside.

4. Mesh sensitivity

Any CFD solution is dependent on the quality of discretization.

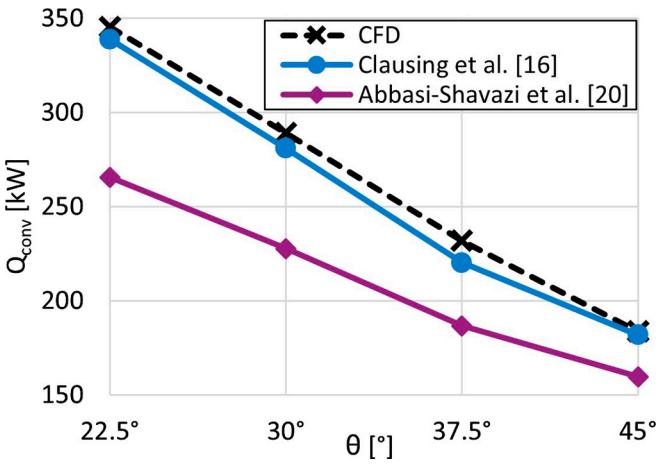


Fig. 6. Free convection (V_{wind} = 0 m/s) from a stationary cavity (ω = 0 rpm).

Meanwhile, the number of elements has to be kept at a reasonable level to minimize the computational effort. We considered not only the number of elements but also their size and distribution and performed a two-stage mesh sensitivity analysis by observing the variation of convective heat loss between different meshes.

In the first stage, we focused on the number of elements in the boundary layer and the thickness of the first element next to a wall in the cavity, expressed in dimensionless wall-normal distance, y^+. The results were indeed insensitive to y^+ as claimed and adding more than 20 elements in the boundary layer did not lead to any significant changes in calculated heat loss values.

The second stage of mesh sensitivity was on the element sizing. We considered both face and volume sizes. Both sizes were observed to have significant effects. In the end, we decided to use the settings yielding a mesh with 3.83·10^6 elements. The cavity faces are discretized with surfaces measuring 0.06 m across. Inflation layer in the cavity has 17 elements with first height of 0.01 m and growth rate of 1.08. Extensive results of the mesh sensitivity study are listed in Appendix A.

5. Verification

Upon scanning the relevant literature, we could not identify any results from experiments performed on a rotating cavity receiver at the relevant Gr and Re ranges. Similarly, existing correlations for the static cavities are derived using data from smaller units [49,50], rendering them unfit for comparison. However, there exists well-established correlations for free convection which are valid in the high-Gr range. Verifying the quality of the free convection simulations ensures that heat transfer to the air from the walls and buoyancy driven flow is modelled correctly, leaving only the interaction of the wind with the cavity unverified. While we expect that the chosen turbulence model will yield results with adequate accuracy based on its performance in modelling various industrial flows, we also acknowledge that this cannot replace a proper verification against relevant experimental data.

Two correlations from Clausing et al. [16] and Abbasi-Shavazi et al. [20] describing natural convection from inclined cavities were selected for verifying the CFD model. Both correlations are well-proven by their authors and the literature following them. The former is valid for the complete Ra range with 3 different sets of coefficients. The latter is derived using data from a smaller unit in ambient air for Gr ∈ [2.63×10^5 – 1.36×10^7] which is below the turbulent regime starting around Ra = Gr•Pr > 10^9. We still considered this correlation because it can represent the effects of tilt on convective losses.

Verification studies were performed on the same geometry and boundaries shown in Figs. 3 and 4. To satisfy the conditions for both correlations, isothermal walls at the average cavity temperature of 1063

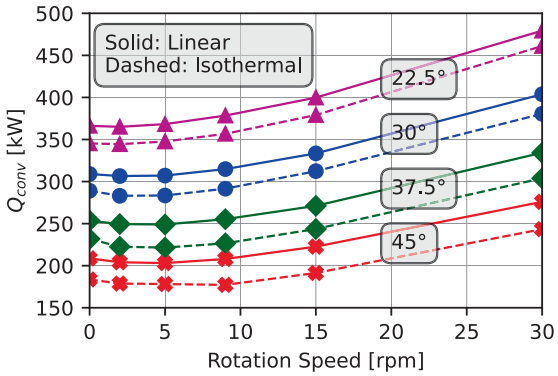


Fig. 7. Free convection losses at different rotation speeds and tilt angles for isothermal (1063 K) or linearly increasing sidewall temperature.

K were assumed. In the results presented in Fig. 6, all four tilt angles listed in Table 1 were considered. CFD results agree well with the correlation from Clausing et al. [16] while the correlation by Abbasi-Shavazi et al. [20] gives estimates 10-20% below CFD results since it does not account for the increased heat transfer due to turbulence. Both correlations confirm the decreasing trend in convective losses with increasing tilt and CFD results show excellent agreement with the model valid in fully turbulent regime.

Furthermore, during the model selection studies, we were able to replicate the experimental results for convective losses from the setup described in [20] within 5% using the same computational model described this manuscript, under Section 3.1. Based on agreement with the correlations and ability to replicate experimental results from the literature, we conclude that the CFD model is accurate when modelling convection from a cavity with significant buoyancy effects.

6. Results

6.1. Free convection from rotating cavity

In order to isolate the effect of rotation from wind, no-wind cases were simulated first. In addition to zero and design rotation speed (30 rpm), four intermediate rotation speeds were also considered to generalize the results. The results are presented in Fig. 7. Here, data connected with dashed lines are obtained by assuming isothermal walls at average particle temperature of 1063 K, as done for the verification simulations. The data connected by solid lines are obtained using the temperature

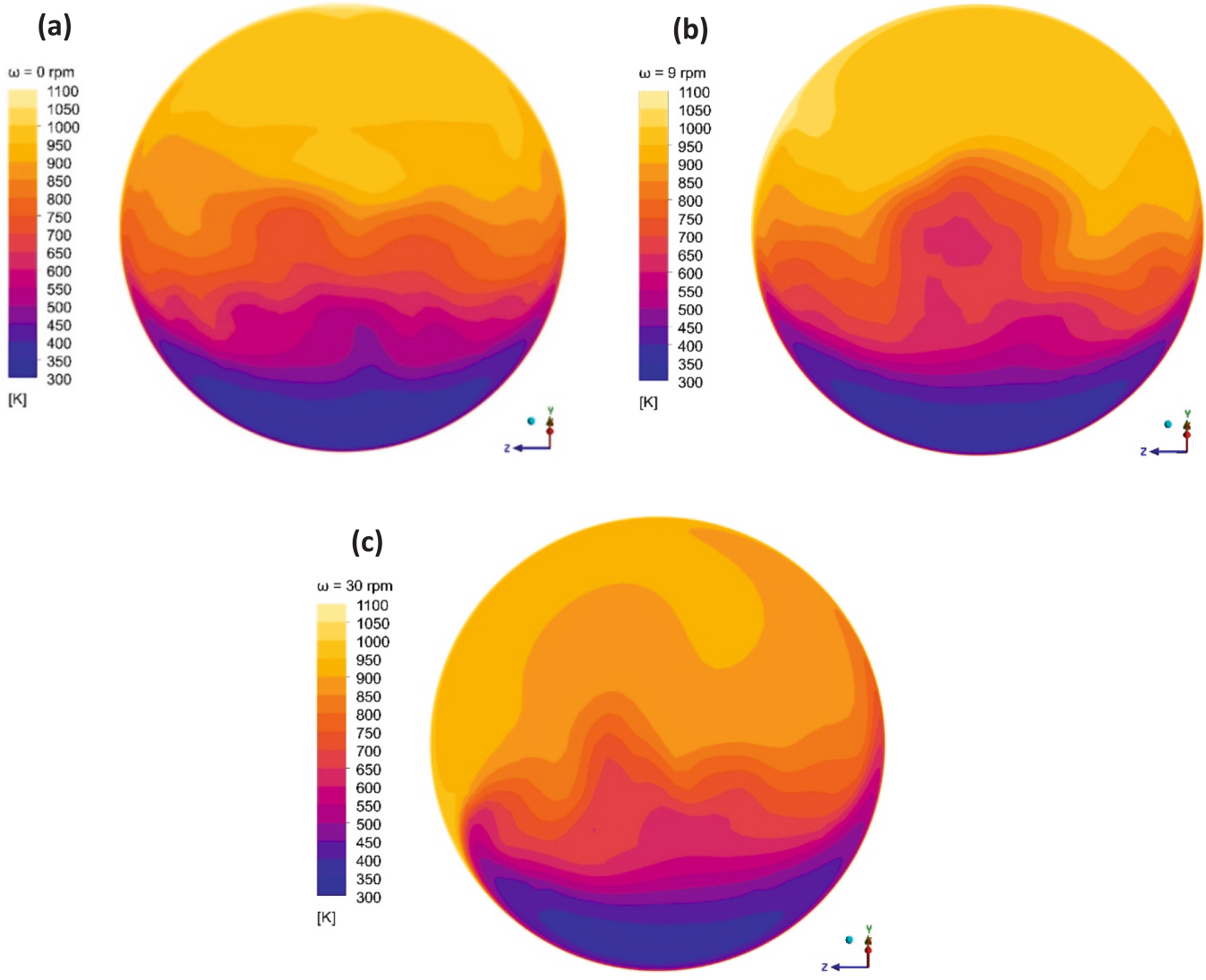


Fig. 8. Cross-Section temperature contours from the mid-length of the receiver for free convection and linearly increasing side wall temperature for $\theta = 30°$. a) $\omega = 0$ rpm, b) $\omega = 9$ rpm, c) $\omega = 30$ rpm CCW.

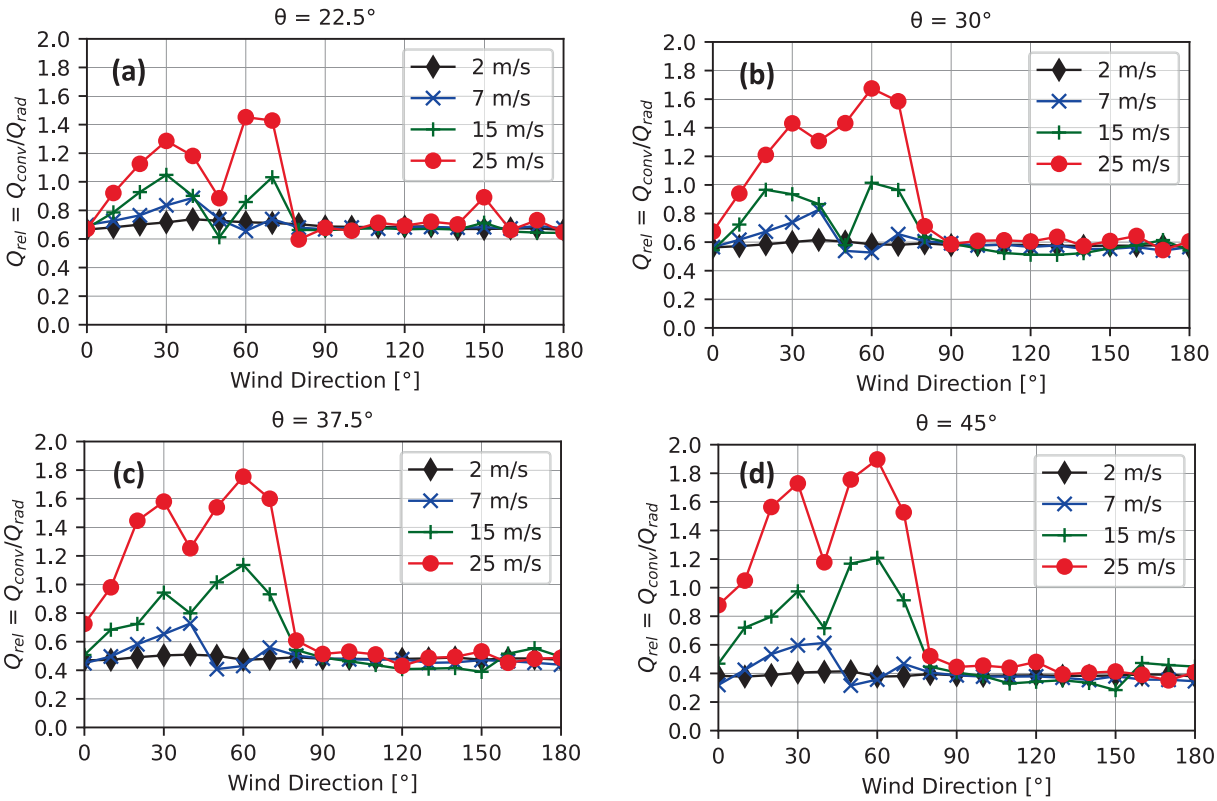


Fig. 9. Normalized convective losses from a CCW rotating receiver for different wind velocities and tilt angles.

boundary conditions described by Eq. (1) and the subsequent paragraph in Section 3.2.

Tilting the receiver down reduces the convective losses for all rotation speeds. Moreover, this does not affect the shape of the curve,

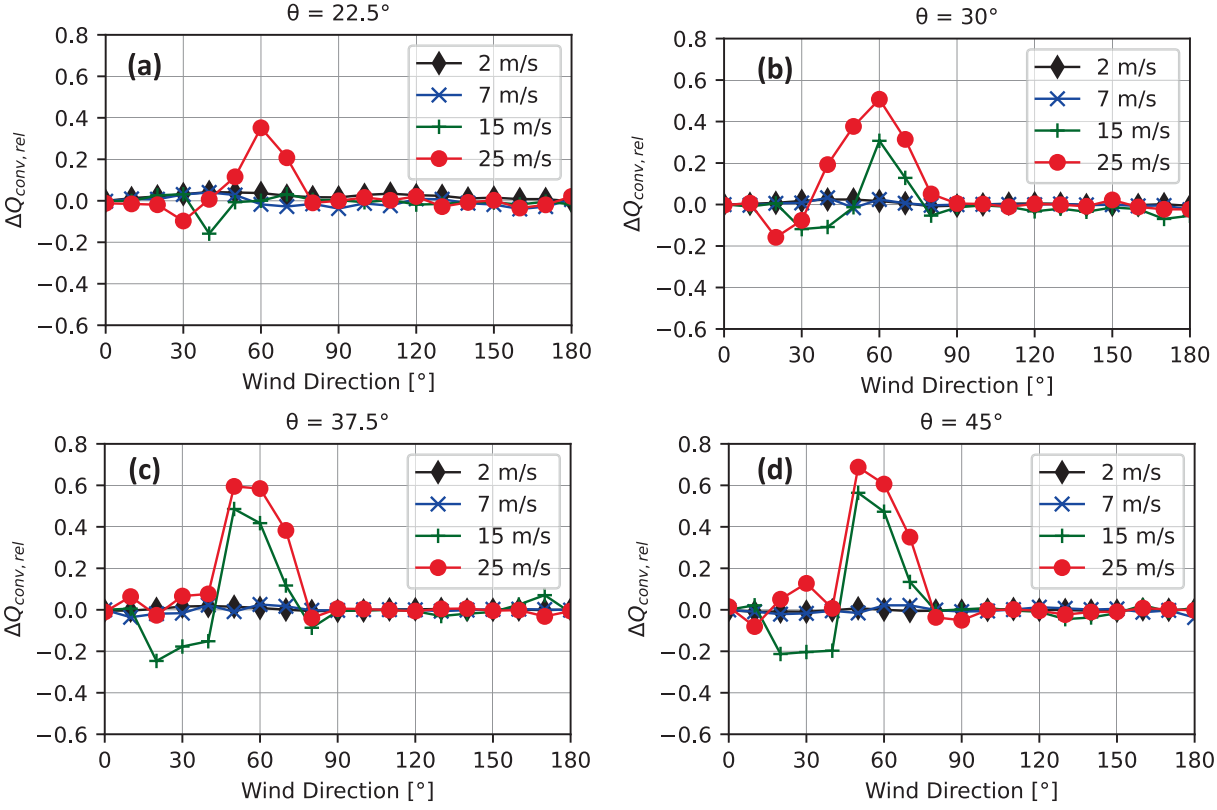


Fig. 10. Difference in convective losses between CCW and CW rotating cavity for different wind velocity and receiver tilt angles.

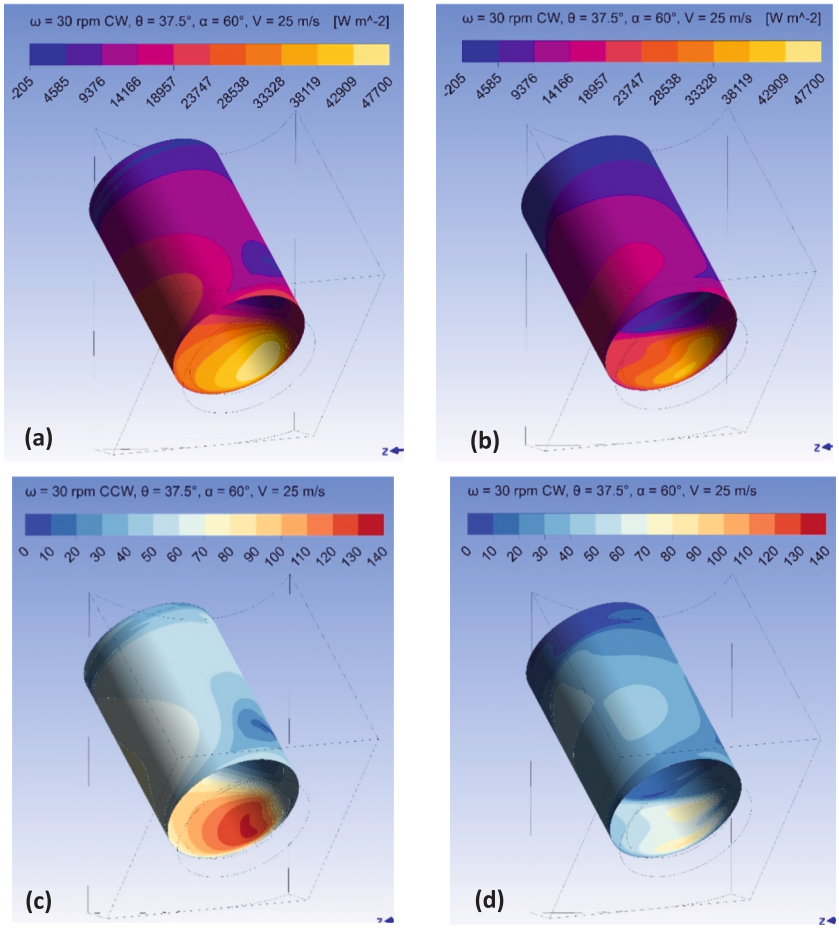


Fig. 11. y^+ and convective heat flux contours for the $\theta = 37.5°$, $\alpha = 60°$, $V_{wind} = 25$ m/s case. a and b) Convective heat flux contours for the CCW (left) and CW (right) rotation, c and d) y^+ contours.

suggesting the effects of tilt and rotation are independent. This is coherent with the findings in the literature for free convection from cavity receivers. Secondly, convective losses change nonlinearly with increasing rotation speed. At low rotation speeds, convective losses drop slightly below no-rotation level and then increase significantly above 10 rpm. Based on these results, we conclude that rotation does not have a significant effect on convective losses below 10 rpm for this receiver, but leads to increased convective losses at normal rotation speed. Also, assuming an average temperature will underestimate convective losses by 10-40 %.

Rotation has two key effects: First, it introduces a resistance for air flow in and out of the cavity as moving walls impart a swirling velocity field to the air in the cavity. Second, it exposes the surfaces shielded under the hot air pocket to cold air. The former effect is dominant in low rotation speeds, even if the low-speed rotation does not produce a meaningful reduction. As the rotation speed increases, cold air is pulled along the rotating wall, touching more of the hot surfaces while hot air from above is pulled down into the convective zone, blurring the distinction between the two zones. Consequently, the air leaving the receiver becomes warmer, increasing convective losses. In Fig. 8, the variation the in cross section temperature field is shown. As ω increases, twisting action becomes clearer.

6.2. *Rotating cavity: wind direction, speed and tilt*

Parallel to the results presented in the literature, wind speed and direction have a significant impact on convective losses as shown in Fig. 9. For some cases, convective losses can almost double the radiative losses while having less but still significant influence for other combinations. Radiative heat loss (Q_{rad}) for all of the cases with the linearly increasing side wall temperature was 0.7 MW. When the wind is barely blowing at 2 m/s, results are quite similar to free convection levels shown in Fig. 4. With increasing θ, convective losses decrease, and no meaningful peaks or valleys are observed as the wind direction changes. At 7 m/s, there is a distinct peak at $\alpha = 40°$, followed by a dip and a second peak around $\alpha = 70°$. Then convective losses level out. At 15 m/s, we again observe double peaks around 30 and 70°, followed by a level-out for back winds. This time, the peaks are much more pronounced and convective loss increases to 1.0 - 1.2 times the radiative losses. When wind picks up at 25 m/s, convective losses increase across all directions, while showing a similar pattern.

An interesting observation concerns the variation of convective losses with θ for slower and faster wind speeds. Slow winds do not change the trend of decreasing losses with increasing θ. At higher wind speeds, however, the convective losses increase with increasing θ, in contrast with free convection. Ri numbers corresponding to these data sets are between [0.093, 0.291], indicating forced convection is dominant. Based on the data in Fig. 9, we conclude that the receiver becomes more susceptible to winds as it is tilted further for the examined range and the peak around 60° becomes more pronounced.

Unlike static receivers, rotation voids the symmetry of the geometry. We covered all significant combinations of wind direction and rotation by reversing the sense of rotation from counterclockwise ($\omega = 30$ rpm), as described in Fig. 1, to clockwise ($\omega = -30$ rpm) for one-half of the possible wind directions ($\alpha \in [0°, 180°]$). A change in the sense of rotation is equivalent to mirroring wind direction with respect to the symmetry plane of the receiver ($\alpha < 0°$). The difference of convective losses between the counterclockwise (Fig. 9) and clockwise rotation

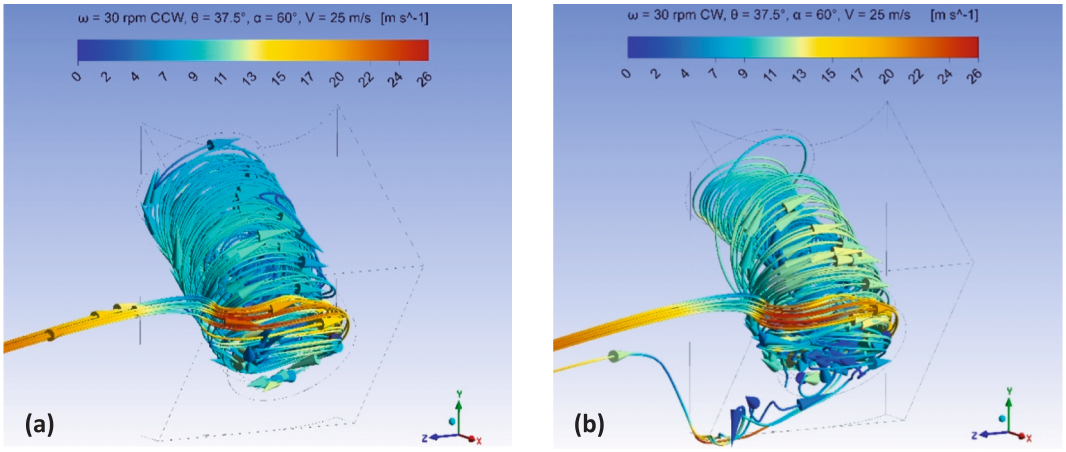


Fig. 12. Streamlines entering the cavity for both a) CCW (left) and b) CW (right) rotation. $\theta = 37.5°$, $\alpha = 60°$, $V_{wind} = 25$ m/s.

($\Delta Q_{rel} = Q_{rel,CCW} - Q_{rel,CW}$) is plotted in Fig. 10.

Changing the sense of rotation does not show any discernible effect for low wind speeds (2 and 7 m/s). Combined with lower overall convective losses, we conclude that the wind does not have enough momentum to affect the stratification in the cavity significantly. Consequently, the problem becomes quasi-symmetric and the variations

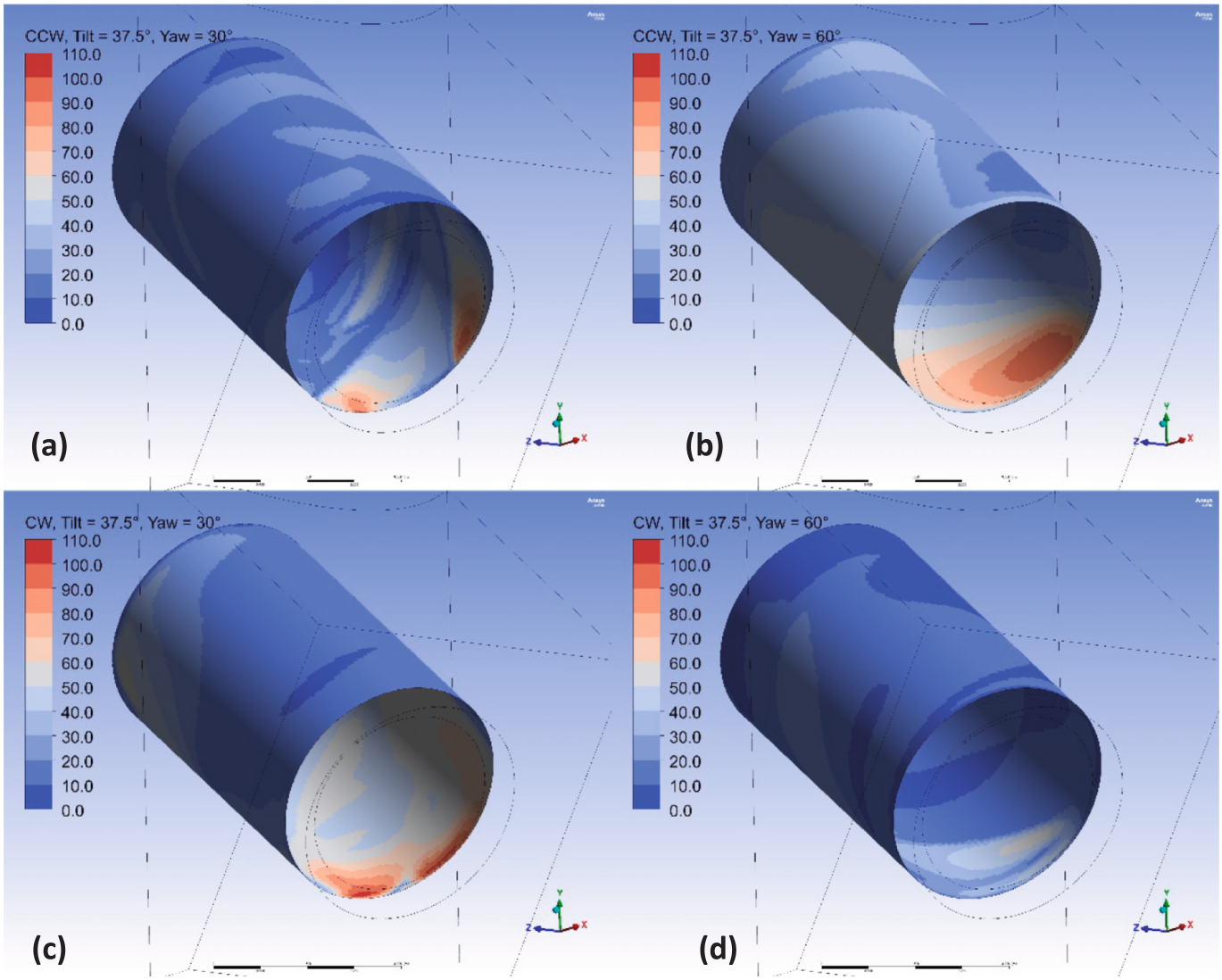


Fig. 13. y^+ values on the cavity side wall for the CCW (a,b) and CW (c,d) rotating receivers tilted by 37.5°, under 15 m/s wind blowing from $\alpha = 30°$ (a,c) and 60° (b,d).

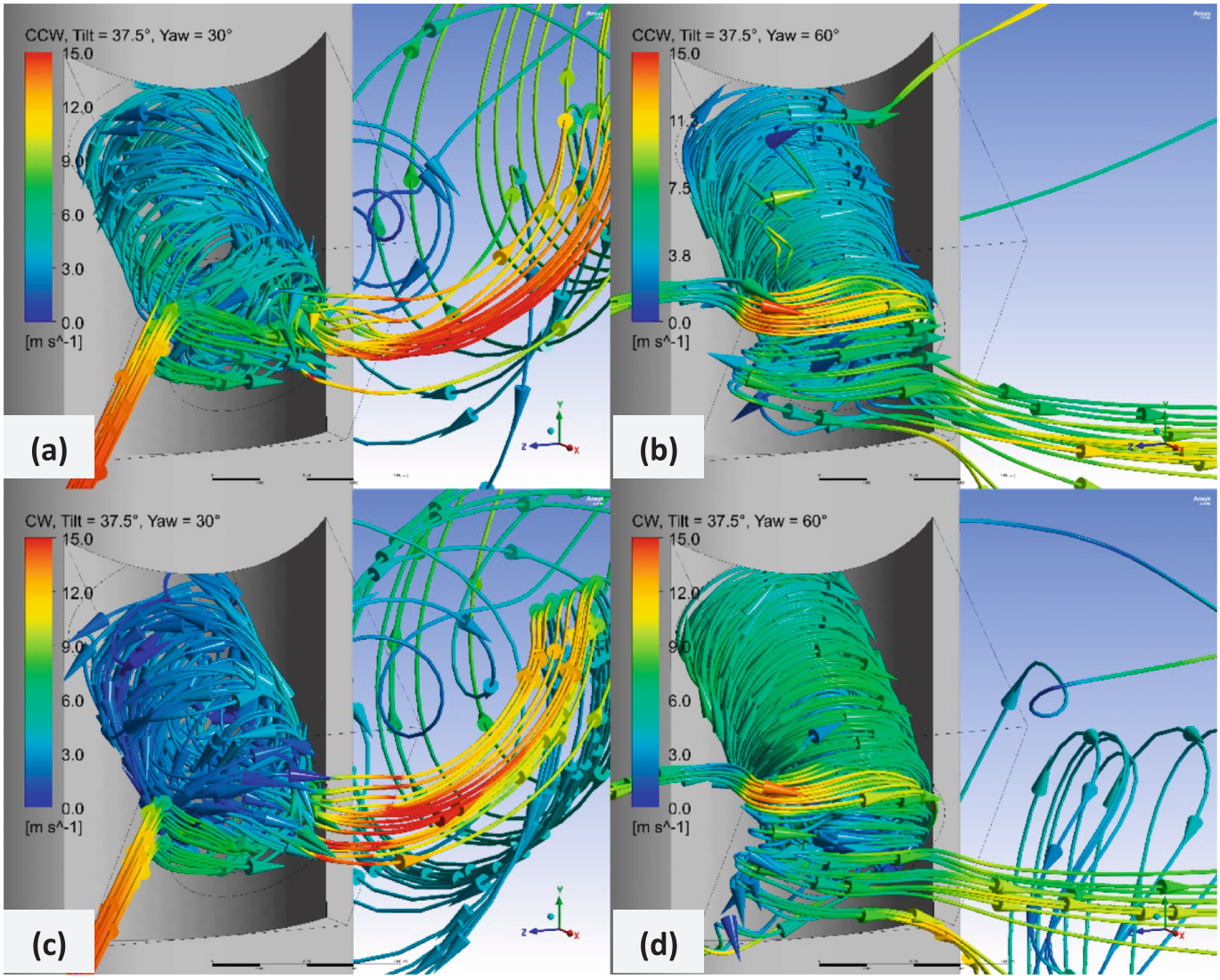


Fig. 14. Streamlines passing the aperture plane for the CCW (a, b) and CW (c, d) rotating receivers tilted by 37.5°, under 15 m/s wind blowing from $\alpha = 30°$ (a, c) and 60° (b, d).

with respect to the wind direction is the same for $\alpha < 0°$ and $\alpha > 0°$. However, as the wind speed increases to 15 and 25 m/s, there are significant differences in convective losses between a clockwise and counterclockwise rotating receiver under the same wind condition.

For $10° < \alpha < 40°$, increasing θ changes the effect of rotation. For the 25 m/s case, when the receiver has a shallower θ, CW rotation reduces convective losses whereas for 45°, it leads to an increase. On the contrary, at 15 m/s wind has a stronger influence when the receiver is rotating clockwise. Front winds are similar to free convection and the sense of rotation does not have an effect on convective losses at all wind speeds. As the wind becomes more sideways, towards the peak around $\alpha = 60°$, we see that sense of rotation can influence convective losses by 50%. Also, both the magnitude of convective losses and difference between two senses of rotation increases as the receiver is tilted further down. For back winds, results show negligible differences for all θ. Overall, we see not only the speed of rotation but also the sense of rotation has a significant effect on convective losses.

In order to understand the differences that rotation causes, local heat flux (positive for outflux) and y^+ values are compared on the cylindrical side wall of the cavity. Fig. 11 shows contours for the second peak of 37.5° tilt, 25 m/s case at $\alpha = 60°$. While the colors in the map are different, heat flux contours closely follow y^+ contours for both cases. Most of the convective heat loss takes place close to the aperture while some portions deep in the cavity have net influx. CCW rotating case with higher convective losses also has higher peak and average y^+ values.

In order to understand how wind enters into the cavity and distributes inside, streamlines in Fig. 12 were plotted for the same case. In both cases, wind enters the cavity from the top right part of the aperture and induces a CW swirl. When the cavity is rotating CCW, this increases the relative velocity magnitude between the wall and the air in the cavity and decreases the boundary layer thickness. Therefore, an increase in y^+ value is observed. Also, streamlines move deeper into the cavity for the CCW rotation, even if the velocity magnitude is less at deeper portions. As a result, convective losses are higher for deeper portions of the cavity as well. On the other hand, clockwise rotation moves the walls in the same direction as the air, reducing velocity difference. This increases the boundary layer thickness, i.e. decreases the gradients of velocity, and temperature. The result is a reduction in heat loss by convection.

At 15 m/s, we observe the same mechanisms in action. This time, however, we focus on how wind direction changes the path of air entering the cavity. In Fig. 13, the y^+ contours for $\alpha = 30°$ and 60° for the same geometry are shown. While we see that the hot spots are located close for both wind directions, the sense of rotation has the opposite effect. Streamlines drawn in Fig. 14 show that the air entering the cavity

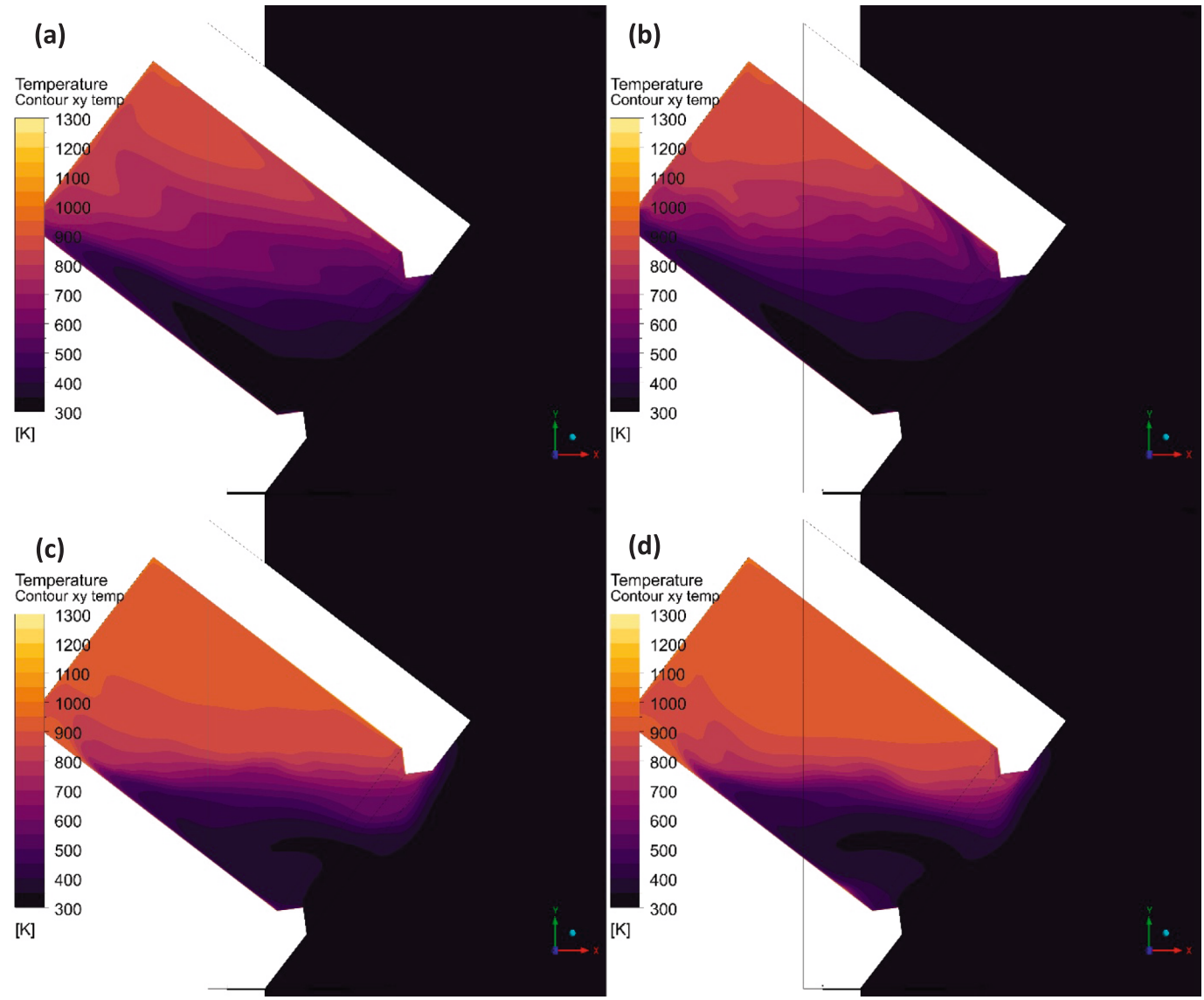


Fig. 15. Temperature contours for the CCW (a, c) and CW (b, d) rotating receivers tilted by 37.5°, under 7 m/s wind blowing from $\alpha = 30°$ (a, b) and 60° (c, d).

induces either clockwise ($\alpha = 30°$) or counterclockwise ($\alpha = 60°$) swirl, regardless of the sense of rotation of the cavity. When the front component of the velocity vector is larger, air follows the tilted radiation shield parallel to the aperture plane from top to bottom. Then the cold air enters the cavity from the bottom-upstream portion and hot air leaves the cavity from the top-downstream corner. When the sideways component is from left to right (when looking into the cavity), air moves CCW in the cavity. On the contrary, when the wind has a stronger sideways component, the point of entry moves to the top-downstream corner and air leaves from the bottom-upstream region and air moves clockwise in the cavity. Same as the 25 m/s case, convective losses are higher when the air circulates in the opposite direction of cavity rotation.

At 7 m/s, streamlines enter the cavity in the ways shown in Fig. 14. However, slower wind speed translates into slower wind-induced flow in the cavity as well. Consequently, the disturbance in the stagnant zone is less. Temperature contours presented in Fig. 15 support this claim. Between 7 and 15 m/s, $Ri = Gr/Re^2$ decreases by a factor of 4.592, indicating a significant transition from a regime where buoyancy has a stronger effect on the flow to a wind-dominated regime. While there are differences in convective losses due to a change in sense of rotation, this is not as visible as it is for higher wind speeds because Ri is between 0.258-0.291 at 15 m/s instead of 1.18-1.34 at 7 m/s. Furthermore, the contours Fig. 15 a and b for $\alpha = 30°$ are darker than c and d for $\alpha = 60°$, showing that the wind increases the convective loss by disturbing the stagnant zone in the receiver. The contours show no discernible difference between counterclockwise (a, c) and clockwise (b, d), in line with results presented in Fig. 10 c.

7. Conclusion

In this paper, the effect of rotation on convective losses from a large-scale receiver has been investigated for free and mixed convection using numerical methods. For free convection, rotation at normal speed increases convective losses up to 25% compared to non-rotating cavities. Thus, the effect of rotation cannot be neglected to estimate heat losses of such a solar receiver correctly. Slow rotation speeds up to 9 rpm reduce convective losses by a negligible amount. Faster rotation increases the convective losses by disturbing the stagnant zone. Walls pull the air close to them and push cold air up into the stagnant zone while dragging hot air down into the convective zone. The effect is quite visible on mid-section temperature contours given in Fig. 8. As the cavity is tilted further, convective losses decrease regardless of rotation speed. Moreover, the temperature distribution on the cavity walls has a significant

effect on convective losses even if the average temperatures are equal. Both correlations used for verification fail to capture this effect.

For very slow wind speeds, no discernible difference from free convection from a rotating receiver has been observed. When wind speed increases to 7 m/s, a variation of convective heat loss with wind direction became visible. The worst direction at $\alpha = 40^{\circ}$ can increase convective losses by 50% above free convection level. Another, albeit small peak exists at $\alpha = 70^{\circ}$. However, the wind is still not too strong to completely disrupt the stagnation zone. At 15 m/s, both peaks become well defined and convective losses increase for all directions for $\alpha < 90^{\circ}$. Faster winds at 25 m/s can increase convective losses up to 1.3 MW, almost twice the radiative losses at 0.7 MW. Interestingly, increasing the tilt increases convective losses for the 15 and 25 m/s cases. Wind has negligible effects for back winds ($\alpha > 90^{\circ}$).

The effect of rotation is different under wind. At slow wind speeds, wind direction or sense of rotation has negligible effect on convective losses. In this regime, the velocity profile is determined by rotation ($V_{wall} = 5.945$ m/s) and wind has less momentum and can penetrate less into the cavity. As wind speed increases, air enters the cavity at speed and introduces a swirl that is independent from rotation. The sense of swirl is a function of the wind direction. If the wind-induced air motion rotates in the opposite sense with respect to the side walls, convective losses can be up to 50% higher than losses when the cavity is rotating in the opposite sense. The highest variation occurs around $\alpha = 60^{\circ}$. Depending on site conditions it might be beneficial to include reversible drives in the design of centrifugal receivers, to reduce convective losses under variable wind directions. Alternatively, the sense of rotation could be selected based on the annual wind data for the site. In any case, penetration of strong winds has to be prevented by using variable strategies addressing different phenomena observed for different wind directions and speeds.

CRediT authorship contribution statement

Onur Polat: Writing – review & editing, Writing – original draft, Visualization, Validation, Methodology, Investigation, Formal analysis. **Luka Lackovic:** Writing – review & editing, Supervision, Project administration, Funding acquisition, Conceptualization. **Reiner Buck:** Writing – review & editing, Supervision, Conceptualization. **Robert Pitz-Paal:** Writing – review & editing, Supervision. **Harald Kruggel-Emden:** Writing – review & editing.

Declaration of competing interest

The authors declare that they have no known competing financial interests or personal relationships that could have appeared to influence the work reported in this paper.

Acknowledgements

The work was made possible with the support of a scholarship from German Academic Exchange Service (DAAD).

Appendix

A – Mesh Sensitivity Study

Table A1
Mesh Sensitivity Study Results (italic = poor; normal = improving; bold and underlined = OK)

Case Name	Best	Finest 3	Finest 2	Ultra-Fine	Finest	Finer	Fine	Mid	Coarse
Cavity face size (across)	0.06	0.06	0.06	0.03	0.06	0.12	0.18	0.24	0.48
Vol. Size (edge)	0.11	0.125	0.19	0.09	0.09	0.09	0.14	0.19	0.38
Wake Size (edge)	0.45	0.52	0.72	0.36	0.36	0.36	0.54	0.72	1.44
Number of Cells [*10^6]	3.83	3.08	2.39	7.00	4.97	4.33	2.14	1.08	0.545
Q_{conv} [kW]	**669.1**	641.6	632.3	**668.2**	**662.9**	638.6	*819.9*	*927.9*	*808.6*
Average y^+ (Cavity)	15.7	15.6	15.4	16	15.6	15-16	23.37	20.92	25.86

Data availability

Data will be made available on request.

References

[1] R. Chen, M. Romero, J. González-Aguilar, et al., Design and off-design performance comparison of supercritical carbon dioxide Brayton cycles for particle-based high temperature concentrating solar power plants, Energ. Conver. Manage. 232 (2021) 113870.
[2] J. Stengler, M. Bülow, R. Pitz-Paal, Concentrating solar technologies for low-carbon energy, Nature Reviews Clean Technology 1 (10) (2025) 719–733.
[3] T. Liu, J. Yang, Z. Yang, et al., Techno-economic feasibility of solar power plants considering PV/CSP with electrical/thermal energy storage system, Energ. Conver. Manage. 255 (2022) 115308.
[4] İ. H. Yılmaz and M. S. Büker, "A critical review of regional dynamics, advances and challenges in concentrating solar technologies in Turkiye," *International Journal of Ambient Energy*, vol. 47, no. 1, 2026.
[5] R. Buck, P. Schwarzbözl, 4.17 Solar Tower Systems, in: *Comprehensive Energy Systems*, Elsevier, 2018, pp. 692–732.
[6] A. Gorjian, E. Rahmati, S. Gorjian, et al., A comprehensive study of research and development in concentrating solar cookers (CSCs): Design considerations, recent advancements, and economics, Sol. Energy 245 (2022) 80–107.
[7] M. Saini, A. Sharma, V.P. Singh, et al., Solar thermal Receivers—A Review, in: P. Verma, O.D. Samuel, T.N. Verma (Eds.), Advancement in Materials, Manufacturing and Energy Engineering, Vol. II, Singapore, Springer Nature Singapore, 2022, pp. 311–325.
[8] R.P. Merchán, M.J. Santos, A. Medina, et al., High temperature central tower plants for concentrated solar power: 2021 overview, Renew. Sustain. Energy Rev. 155 (2022) 111828.
[9] M. Imran Khan, F. Asfand, S.G. Al-Ghamdi, Progress in technology advancements for next generation concentrated solar power using solid particle receivers, Sustainable Energy Technol. Assess. 54 (2022) 102813.
[10] L. Yue, N. Schroeder, C.K. Ho, Particle Flow Testing of a Multistage Falling Particle Receiver Concept: Staggered Angle Iron Receiver (STAIR), American Society of Mechanical Engineers, 2020.
[11] J.-S. Kim, W. Gardner, D. Potter, et al., in: Design of a Multi-Stage Falling Particle Receiver with Truncated-Cone Geometry, AIP Publishing, 2020, p. 30023.
[12] M. Lubkoll, M. Ebert, L. Amsbeck, et al., Development Progress of the CentRec® Particle Receiver Technology, AIP Publishing, 2022.
[13] W.P. Breugem, B.J. Boersma, R.E. Uittenbogaard, The influence of wall permeability on turbulent channel flow, J. Fluid Mech. 562 (2006) 35–72.
[14] M.E. Rosti, L. Cortelezzi, M. Quadrio, Direct numerical simulation of turbulent channel flow over porous walls, J. Fluid Mech. 784 (2015) 396–442.
[15] A.M. Clausing, An analysis of convective losses from cavity solar central receivers, Sol. Energy 27 (4) (1981) 295–300.
[16] A.M. Clausing, J.M. Waldvogel, L.D. Lister, Natural Convection from Isothermal Cubical Cavities with a Variety of Side-Facing Apertures, J. Heat Transfer 109 (2) (1987) 407–412.
[17] A.M. Clausing, L.D. Lister, J.M. Waldvogel, Combined convection from isothermal cubical cavities with a variety of side-facing apertures, Int. J. Heat Mass Transf. 32 (8) (1989) 1561–1566.

[18] U. Leibfried, J. Ortjohann, Convective Heat loss from Upward and Downward-Facing Cavity Solar Receivers: Measurements and Calculations, J. Sol. Energy Eng. 117 (2) (1995) 75–84.
[19] T. Taumoefolau, S. Paitoonsurikarn, G. Hughes, et al., Experimental Investigation of Natural Convection Heat loss from a Model Solar Concentrator Cavity Receiver, J. Sol. Energy Eng. 126 (2) (2004) 801–807.
[20] E. Abbasi-Shavazi, J.F. Torres, G. Hughes, et al., Experimental correlation of natural convection losses from a scale-model solar cavity receiver with non-isothermal surface temperature distribution, Sol. Energy 198 (2020) 355–375.
[21] R.K. McMordie, Convection Heat loss from a Cavity Receiver, J. Sol. Energy Eng. 106 (1) (1984) 98–100.
[22] M. Pavlović, F. Penot, Experiments in the mixed convection regime in an isothermal open cubic cavity, Exp. Therm Fluid Sci. 4 (6) (1991) 648–655.
[23] B. Mills, R. Shaeffer, C.K. Ho, et al., Modeling the Thermal Performance of Falling Particle Receivers Subject to External Wind, American Society of Mechanical Engineers, 2019.
[24] J.B. Fang, J.J. Wei, X.W. Dong, et al., Thermal performance simulation of a solar cavity receiver under windy conditions, Sol. Energy 85 (1) (2011) 126–138.
[25] P. Liovic, J.-S. Kim, G. Hart, et al., Wind dependence of energy losses from a solar gas reformer, Appl. Therm. Eng. 63 (1) (2014) 333–346.
[26] T. Tan, Y. Chen, Z. Chen, et al., Wind effect on the performance of solid particle solar receivers with and without the protection of an aerowindow, Sol. Energy 83 (10) (2009) 1815–1827.
[27] R. Flesch, H. Stadler, R. Uhlig, et al., On the influence of wind on cavity receivers for solar power towers: an experimental analysis, Appl. Therm. Eng. 87 (2015) 724–735.
[28] S. Siegrist, H. Stadler, B. Hoffschmidt, Wind tunnel measurements of forced convective heat loss from multi-megawatt cavities of solar central receiver systems, Sol. Energy 169 (2018) 607–615.
[29] Z. Wan, J. Wei, J. Su, et al., Convective heat loss under windy conditions and effects of porous shroud for large scale cavity receiver, Sol. Energy 286 (2025) 113202.
[30] C.K. Ho, J. Sment, K. Albrecht, et al., Gen 3 Particle pilot Plant (G3P3) – High-Temperature Particle System for Concentrating Solar Power (Phases 1 and 2), Sandia National Laboratories (2021).
[31] W. Wu, L. Amsbeck, R. Buck, et al., On the influence of rotation on thermal convection in a rotating cavity for solar receiver applications, Appl. Therm. Eng. 70 (1) (2014) 694–704.
[32] Bundesrepublik Deutschland, "Straßenverkehrs-Zulassungs-Ordnung (StVZO): § 32 Abmessungen von Fahrzeugen und Fahrzeugkombinationen," https://www.gesetze-im-internet.de/stvzo_2012/_32.html.
[33] Don-Bur (Bodies & Trailers) Ltd., "Understanding Bridge Height Restrictions for HGVs," https://donbur.co.uk/faqs/safety/bridge-height-restrictions-hgv.html.
[34] B. Gobereit, L. Amsbeck, R. Buck, et al., Assessment of a falling solid particle receiver with numerical simulation, Sol. Energy 115 (2015) 505–517.
[35] R. Uhlig, R. Flesch, B. Gobereit, et al., Strategies Enhancing Efficiency of Cavity Receivers, Energy Procedia 49 (2014) 538–550.
[36] F.R. Menter, Two-equation eddy-viscosity turbulence models for engineering applications, AIAA J. 32 (8) (1994) 1598–1605.
[37] F.R. Menter, Review of the shear-stress transport turbulence model experience from an industrial perspective, International Journal of Computational Fluid Dynamics 23 (4) (2009) 305–316.
[38] Menter, F. R., Kuntz, M., Langtry, R., "Ten Years of Industrial Experience with the SST Turbulence Model," *Turbulence, Heat and Mass Transfer*, vol. 4, 2003.
[39] ANSYS Inc., "Fluent Theory Guide, Release 2024 R2," https://ansyshelp.ansys.com/public/account/secured?returnurl=////Views/Secured/corp/v242/en/flu_th/flu_th.html.
[40] W.M. Haynes, D.R. Lide, T.J. Bruno, *CRC Handbook of Chemistry and Physics*, CRC Press, 2016.
[41] E. Johnson, S. Hicdurmaz, R. Buck, et al., Beam radiation penetration in particle beds for heat transfer modeling of a centrifugal solar particle receiver, J. Quant. Spectrosc. Radiat. Transf. 295 (2023) 108403.
[42] C. Chen, C. Yang, D. Ranjan et al., "Spectral Radiative Properties of Ceramic Particles for Concentrated Solar Thermal Energy Storage Applications," *International Journal of Thermophysics*, vol. 41, no. 11, 2020.
[43] J. Grobbel, *Modeling Solar Particle Receivers with the Discrete Element Method*, Ph.D, RWTH Aachen 12 (2019) 12.
[44] CARBO Ceramics Inc., "CARBOBEAD HTM: High-performance ceramic heat transfer media to enhance efficiencies in renewable energy systems," https://carbo.tech/wp-content/uploads/2024/11/CARBOBEAD_HTM-TDS.pdf.
[45] Wu. Wei, *A Centrifugal Particle Receiver for High-temperature Solar applications*, Ph.D, RWTH Aachen, 2015.
[46] L. Yue, B. Mills, J. Christian et al., "Effect of Quartz Aperture Covers on the Fluid Dynamics and Thermal Efficiency of Falling Particle Receivers," *Journal of Solar Energy Engineering*, vol. 144, no. 4, 2022.
[47] K. Lin, S. Chen, Y. Zeng, et al., Hierarchically structured passive radiative cooling ceramic with high solar reflectivity, Science (New York, N.Y.) 382 (6671) (2023) 691–697.
[48] T.L. Bergman, F.P. Incropera, *Fundamentals of heat and mass transfer*, Wiley, Hoboken NJ, 2011.
[49] S. Siegrist, *Forced Convective Heat loss from Cavities of Multi-Megawatt Scale Solar Receivers*, Ph.D, RWTH Aachen 31 (October 2018).
[50] R. Flesch, H. Stadler, R. Uhlig, et al., Numerical analysis of the influence of inclination angle and wind on the heat losses of cavity receivers for solar thermal power towers, Sol. Energy 110 (2014) 427–437.